Precursor-mediated adsorption of oxygen on the (111) surfaces of platinum-group metals

A. Eichler, F. Mittendorfer, and J. Hafner
Institut für Materialphysik and Center for Computational Materials Science, Universität Wien, Sensengasse 8/12, A-1090 Wien, Austria
(Received 7 December 1999; revised manuscript received 12 April 2000)

The dissociative adsorption of oxygen on the (111) surfaces of platinum, palladium, and nickel has been investigated using *ab initio* local-spin-density calculations. For all three surfaces, adsorption is shown to be precursor-mediated and the structural, energetic, vibrational and electronic properties of the precursors are in very good agreement with the available experimental information. The investigation of the transition states shows that on Pt and Pd the barriers for dissociation are comparable to (or at sufficiently high coverage even higher than) the desorption barriers. In combination with large energies for atomic adsorption, this also leads to a high barrier for associative desorption—in agreement with observation. In contrast, the dissociation barrier for O_2 on Ni(111) is low and occurs already for a less stretched molecule. The trends in molecular and atomic adsorption and in the dissociation barriers are discussed in relation to the geometric and electronic properties of the substrate and to the sticking probabilities observed in molecular-beam experiments.

I. INTRODUCTION

One of the main fields of interest in modern surface science is gas-surface interactions with a background of catalysis.[1] Since all chemical reactions at surfaces are based on adsorption and dissociation processes, a detailed knowledge in this field is the foundation for the understanding of more complicated surface reactions. From an experimental point of view, there are two complementary ways to access this problem. On the one hand, stable adsorption structures can be characterized based on the results of spectroscopy and scattering experiments. On the other hand, molecular-beam experiments combined with desorption studies reveal the energy/temperature dependence of the adsorption process. For a microscopic description of the adsorption/dissociation process, experimentalists have to rely on models based on rather simplistic low-dimensional potential surfaces.

During the past few years, theoretical techniques have made increasing contributions in this field. While *ab initio* density-functional-theory (DFT) calculations can determine the potential-energy surface (PES) at least for the adsorption of simple molecules such as H_2,[2–4] O_2,[5,6] or CO (Refs. 7–9) with high accuracy, (quantum) molecular-dynamics simulations using these potential-energy surfaces link the total-energy calculations with macroscopic properties such as sticking coefficients[10,11] or desorption spectra.[12]

Modifying the specific features of the PES helps to understand the relation between the static PES and the dynamic adsorption process. While originally a decrease of the sticking coefficient with increasing beam energy at low energies has always been explained by precursor-mediated adsorption, in which the molecule is trapped before it is finally dissociated and adsorbed,[13] a new mechanism has been found based on theoretical investigations: the so-called steering effect. A slow molecule impinging on an unfavorable orientation can adapt its orientation, so that it has to overcome only the minimal barrier to dissociation and adsorb. For higher energies, the molecule is too fast for such a reorientation mechanism to work, so that the molecule is repelled because of an unfavorable orientation. For H_2, steering dominates the adsorption process, and so far no real precursor states could be identified for hydrogen adsorption. For heavier molecules such as O_2, the experimental predictions of precursor states could be verified by DFT calculations for Ag(110),[6] Pt(111),[5] Pd(111),[14] Cu(110),[15] and Ni(111).[16] The aim of this study is to present a detailed analysis of oxygen adsorption on the (111) surfaces of the metals of the platinum group Ni(111), Pd(111), Pt(111), focusing on the molecular precursor states and the dissociation process. Furthermore, the possible influence of the ferromagnetism of the substrate in the case of adsorption on nickel is investigated.

Our paper is organized as follows. In the following section the experimental situation for the three systems is compiled. In Sec. III we give the details of the calculations upon which our study is based. Sections IV–VI summarize our results on the adsorption of atomic and molecular oxygen on the (111) surfaces of platinum, nickel, and palladium. A comparison/discussion of the adsorption behavior of the investigated surfaces follows in Sec. VII. Finally, we close our paper with a summary of our results.

II. EXPERIMENTS

For the adsorption of oxygen on platinum (111) photoemission spectroscopy of valence states[17,18] and core levels,[19,20] electron energy loss spectroscopy (EELS),[18,21,22] thermal desorption spectroscopy (TDS),[17,21,23,22] and near-edge x-ray-absorption spectroscopy (NEXAFS) (Refs. 24–26) have distinguished a physisorbed state and molecular as well as atomic chemisorbed phases (see Tables I and II).

While there is general agreement that during the chemisorption process charge transfer from the substrate to the molecular $1\pi_g$ orbital of the adsorbate leads to a profound modification of the molecular bond, there is disagreement on the precise nature of the chemisorbed molecular state: while the EELS results have first been interpreted in terms of a nonmagnetic peroxolike O_2^{2-} phase, a paramagnetic superoxolike O_2^{-} state has been postulated on the basis of the NEXAFS data.[25] EELS studies[18,21] have also revealed the existence of two different O-O stretching frequencies, and

TABLE I. Adsorption of atomic oxygen in various high-symmetry sites of Pt(111) at $\Theta = 0.5$ in comparison with experiment: Energy E (eV) of two oxygen atoms with respect to the free O_2 molecule, height above the surface Z (Å) and vibrational frequency ν (cm^{-1}) in wave numbers. The experimental data are taken from Refs. 18,22,27, and 50.

		Top	Bridge	hcp	fcc	fcc (Expt.)
E	(eV)	+0.30	−0.57	−0.98	−1.65	
Z	(Å)	1.85	1.41	1.25	1.23	1.21±0.03
ν	(cm^{-1})	660	540	500	470	466–480

the possible coexistence of two different chemisorbed molecular species is also supported by different core-level spectroscopies.[20] The two different chemisorbed states have been interpreted as due to adsorption at steps or due to two different adsorption sites. A common conclusion of all these studies is that dissociation of O_2 on Pt(111) is a thermally activated process that occurs at $T > 150$ K via a molecular precursor (or molecular precursors) [which is also supported by the measured sticking behavior (Ref. 23 and Fig. 1)] and that atomic oxygen is adsorbed in the threefold hollows. For this atomic phase LEED experiments[27] have determined also the substrate relaxation with high accuracy.

In agreement with a recent scanning tunneling microscopy (STM) study,[28] we identified in a previous study[5] two distinct molecular precursors. One is in a paramagnetic superoxostate, formed at the bridge site with the oxygen atoms oriented towards the on-top sites. The second precursor is in a nonmagnetic peroxostate and located in a slightly tilted position over a hollow site.

For the O_2-Ni(111) system, much less information is available in the literature. Most studies deal with the adsorption of atomic oxygen on the surface, including a LEED experiment[29] and a NEXAFS study.[30] According to those, oxygen adsorbs in the fcc-hollow positions with a Ni-O distance of 1.85 Å.[31] The adsorption energy for atomic oxygen on nickel(111) has been determined by microcalorimetry to be 0.8 eV.[32] Furthermore, a work-function change of 0.82 eV upon adsorption of 0.25 ML oxygen has been observed.[32] Recently a molecular-beam experiment[33] (cf. Fig. 1) postulated a precursor mediated adsorption process similar to that on Pt(111).

TABLE II. Adsorption of molecular oxygen on Pt(111) in comparison with experiment: Sites, bond lengths d in Å and frequencies (symmetric stretch frequency of the molecule ν_1 and metal oxygen frequency ν_2) in wave numbers. Also included are results for the free molecule. The experimental data is taken from Refs. 18,20,21,26,28,50, and 51.

		Site	d (Å)	ν_1 (cm^{-1})	ν_2 (cm^{-1})
free mol.	calc.		1.24	1550	
	exp.		1.21	1580	
mol. prec. 1	calc.	t-fcc-b	1.43	690	340
	exp.	t-fcc-b	1.40–1.47	690–700	?
mol. prec. 2	calc.	t-b-t	1.39	850	370
	exp.	t,b	1.37–1.39	860–875	375–380

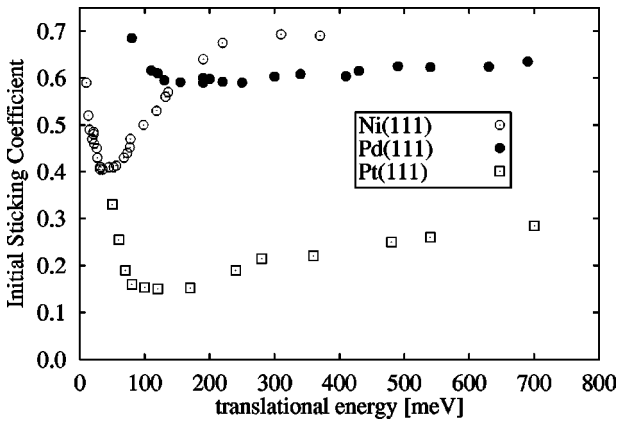

FIG. 1. Initial sticking coefficient for O_2 adsorption as a function of the translational energy. Values are taken from Refs. 33 (Ni, $T_{surf} = 123$ K), [35] (Pd, $T_{surf} = 100$ K), and Ref. 23 (Pt, $T_{surf} = 200$ K).

For palladium, experiments predict an even more complex adsorption mechanism consisting of a system of a physisorbed and up to three molecular precursor states.[34] Again, the sticking curve[35] (cf. Fig. 1) exhibits the typical shape for a precursor-mediated adsorption.

III. METHODOLOGY

Our calculations have been performed using a spin-polarized version of the Vienna *ab initio* simulation program VASP.[36,37] VASP performs an iterative solution of the Kohn-Sham equations of local-spin-density-functional (LSDF) theory via a minimization of the norm of the residual vector and optimized charge- and spin-density mixing routines. The spin-polarized version of VASP (Ref. 38) has been used to account for the magnetic moment of the O_2 molecule and in the case of Ni for the ferromagnetic character of the substrate. The PW91 generalized gradient correction[39] has been used.

Ultrasoft pseudopotentials[40] are used for the description of the electron-ion interaction. The close similarity between the ultrasoft pseudopotential (US-PP) method with the projector-augmented-wave (PAW) technique[41,42] allows us to demonstrate that the accuracy of US-PP calculations using a plane-wave basis equals—except in a few special circumstances—that achieved using the most advanced all-electron techniques. For all Pt-group metals, the use of US-PP's allows us to restrict the basis set to plane waves with a maximum kinetic energy of $E_{cut} = 300$ eV. For any further technical aspects of VASP, see Ref. 37; for details in the construction of the US-PP we refer to our earlier work on Pt, Pd,[43] and Ni (Ref. 44) surfaces.

The substrates are modeled by a four-layer slab with a rectangular $\sqrt{3} \times 2$ unit cell [leading to a $c(4 \times 2)$ structure, cf. Fig. 2], separated by a 14-Å -thick vacuum layer. One oxygen molecule is adsorbed on both sides of the slab resulting in an atomic coverage of $\Theta_O = 0.5$. Brillouin-zone integrations have been performed on a grid of $(3 \times 4 \times 1)$ $\vec{k}$ points, using a Methfessel-Paxton smearing[45] of $\sigma = 0.2$ eV. All calculations have been performed at the equilibrium lattice constants [$a^{Ni} = 3.53$ Å, $a^{Pd} = 3.96$ Å, $a^{Pt} = 3.99$ Å; experimentally: $a^{Ni} = 3.52$ Å, $a^{Pd} = 3.89$ Å, $a^{Pt} = 3.92$ Å] calculated using the gradient-corrected functional.

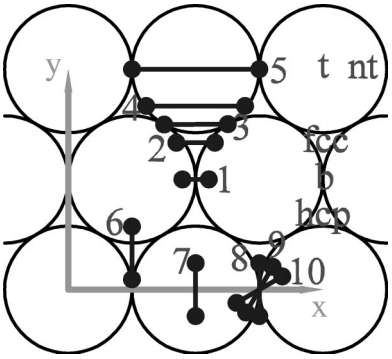

FIG. 2. Surface cell and geometry of the reaction channels explored for O_2 adsorption on Pt(111) via elbow-plots (Figs. 3 and 4), together with a short-hand notation for special points. See the text.

Substrate relaxation effects have been neglected since in our preceding calculations for the adsorption of O_2 on Pt(111) (Ref. 5) and CO on Rh(100) (Ref. 8) and Pd(100) (Ref. 7) we found only a minor influence of the substrate relaxation on the energetics (<100 meV) and geometry of the adsorbate (<0.1 Å).

Results for the free molecule are compiled in Table II. The problematic description of the O_2 bond energy ($E_{O_2}^{GGA}=5.87$ eV, $E_{O_2}^{exp.}=6.2$ eV) stems mainly from the error in the energy of the free atoms. However, since the density gradients are much lower for the adsorption systems, the description of the energy differences between the adsorbed molecule, the transition state, and the adsorbed atoms is much more accurate than the absolute values.

For results on the clean Ni surfaces, we refer to our previous publication.[44]

All energies given in this paper are potential energies with respect to the free O_2 molecule, where the energy zero is set to the free molecule. More formally,

$$E=E(\text{subst}+n\times\text{O})-E(\text{subst})-\frac{n}{2}E(\text{O}_2),$$

where n is the number of oxygen atoms in our cell.

To determine the dissociation barriers, the transition states (TS) have been determined using the nudged elastic band method (NEB).[46,47] In this method, the total energies of a series of intermediate states distributed along the reaction path connecting the starting and final states are simultaneously minimized restricting the atomic motions to the hyperplane perpendicular to the reaction path. We have used this method already successfully to determine diffusion barriers for CO on Pd(100) (Ref. 7) and Rh(100) (Ref. 8) and for the calculation of reaction barriers in the CO oxidation reaction on Pt(111).[48]

IV. OXYGEN ON PLATINUM(111)

The potential-energy surface for the dissociative adsorption of a diatomic molecule over a surface (when neglecting relaxation effects) is six-dimensional. To map such energy surfaces, the common strategy is to compute two-dimensional cuts through the energy surface, so-called elbow plots; the two angles and the two lateral coordinates are fixed and only the bond length of the molecule and its height above the surface (Z) are varied. Within this restricted PES, the evolution of the O_2 molecule can be traced from the molecular phase in the entrance channel through possible molecular precursor states (or transition states) to the final atomic adsorbed O-Pt structures.

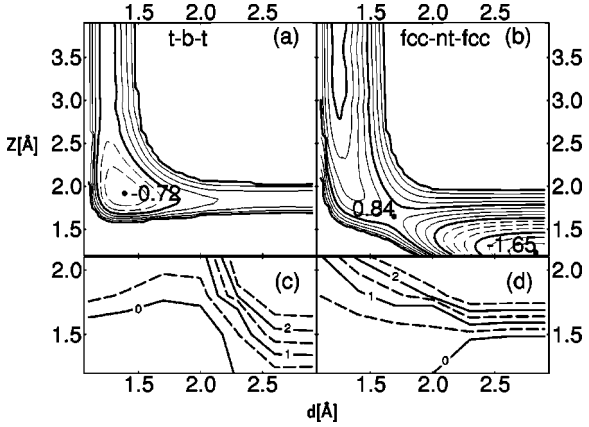

FIG. 3. Contour graph for the potential energy of an O_2 molecule over a Pt(111) surface as a function of the bond length (d) and the height of the molecule above the surface (Z) impinging in a t-b-t (a) and fcc-nt-fcc (b) geometry (pathways 1 and 4 in Fig. 2). Contour lines are drawn in intervals of 0.25 eV, thick full lines correspond to integer values (n eV), dashed lines to negative potential energies. In panels (c) and (d) the variation of the total magnetic moment of the O_2-Pt system is illustrated for the same geometries.

Since we performed for O_2 on platinum a rather extensive investigation based on these so-called elbow plots (see Sec. IV B and Fig. 3), we took also the results presented in the following section for atomic adsorption out of those 2D scans and did no structural relaxation.

A. Atomic adsorption

Figure 2 shows the surface cell and defines a short-hand notation for special points in the surface cell (t, on top; b, bridge; fcc, hcp, threefold hollows; nt, ''near top'') and for the reaction channels used for the investigation of the molecular adsorption.

The adsorption energy is largest in the fcc hollows ($E=-1.65$ eV/molecule) and considerably smaller in the hcp hollows ($E=-0.98$ eV/molecule), Comp. Table I.

This rather large energy difference at such similar surface sites has been interpreted by Feibelman[49] in terms of frustrated d orbitals: due to adsorption, charge is transferred to the oxygen atom leading to a repulsion between the metal d orbitals and the oxygen atom and hence to a deformation of the substrate d orbitals. Since in the Pt-d band only the highest (antibonding) states are unoccupied, charge donation is equivalent to bond weakening. Due to the different symmetry, this leads in the case of hcp adsorption to a weakening of all surface-subsurface bonds, whereas for the fcc hollow one bond out of three is strengthened. This explains the preference for the fcc site. We shall return to a discussion of these charge-redistribution effects in connection with a detailed discussion of the electronic structure of the adsorbates (see Sec. IV C 2 for Pt and Sec. V A, Fig. 10 for Ni).

The characteristic metal-oxygen stretching frequency for the atomic adsorbate is in the fcc-hollow $\nu=470$ cm^{-1}, to

compared with experimental values of $\nu = 466\ \mathrm{cm}^{-1}$, Ref. 22; $\nu = 471\ \mathrm{cm}^{-1}$, Ref. 50; $\nu = 480\ \mathrm{cm}^{-1}$, Ref. 18.

The comparison of our calculated value for the atomic adsorption with the corresponding experimental value from Ref. 22 is difficult, since in these TDS experiments only the effective barrier for oxygen desorption could be determined, which includes in addition to the pure adsorption energy also a possible barrier for the recombination of the O_2 molecule. For this barrier, Parker *et al.*[22] obtained in the coverage range of 0.42–0.5 ML a value between 1.22 and 1.65 eV per O_2 molecule. This large fluctuation has been explained in terms of a pronounced kinetical hindering of the O_2 molecules at the surface, rather than by a variation of the chemical barrier.

Adsorption on bridge and on-top sites is higher in energy, on-top even endothermic. The height above the surface follows the trend in the energies: the more stable the adsorption site, the higher coordinated the site and therefore, at a similar Pt-O bond-length, the smaller the adsorption height. The vibrational frequencies are determined by the geometry of the adsorption site: it is lowest for the fcc hollow, where the molecule can vibrate vertically without any hindrance; in the hcp hollow, the subsurface platinum leads to a slight increase in frequency, whereas on the bridge and especially in the on-top site the stretching frequencies are much higher.

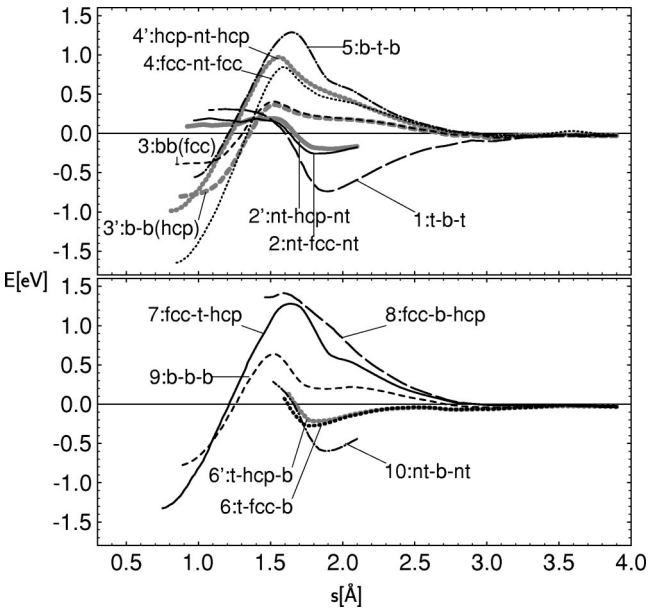

FIG. 4. Adsorption of O_2 on Pt(111): Variation of the potential energy along the bottom of the fourteen reaction channels defined in Fig. 2 and in the text. The reaction coordinate s measures the distance from the starting point 4 Å above the surface plane along the deepest points in each channel.

B. Potential-energy surface

To distinguish between the different geometries with the molecule parallel to the surface, we will characterize them by the positions where the dissociated oxygen atoms will be adsorbed and by the center of mass of the molecule. For example, *h-b-h* refers to a geometry with the center of mass over a bridge position and the atoms oriented towards the fourfold hollows in which they will finally be adsorbed. *h-t-h* leads to the same final positions of the O atoms, but the molecule enters the reaction path over an on-top (*t*) position.

Channels 1 to 5, together with the channels $2'$ to $4'$ located around the hcp instead of the fcc hollow, explore the variation of the potential energy (PE) as a function of the coordinates x,y in the surface cell (see Fig. 2). The dependence of the PE on rotations parallel to the surface is tested in channels 5 and 7 for rotations around the top sites, in channels 2 and 6 ($2'$ and $6'$) around the fcc (hcp) hollows, and in channels 1,8,9,10 for rotations over the bridge sites. Because of symmetry in all these fourteen reaction channels except channels 6,6′, the PE is stationary with respect to a tilting of the molecule out of a plane parallel to the surface. Close to the local minimum of the PE, we have relaxed all six degrees of freedom of the O_2 molecule. Figure 3 shows typical elbow plots, as they are described in the introduction of this section. Panel (a) shows the variation of the energy along the *t-b-t* path (channel 1): the molecule enters the elbow from the upper corner at a height of about 4 Å with a bond length of $d = 1.24$ Å , and a stretching frequency of 1580 wave numbers (curvature in the d direction). From thereon, the energy decreases leading to a local minimum with $E = -0.72$ eV at a distance of $Z = 1.92$ Å and a bond length of $d = 1.39$ Å . A further elongation of the molecule raises the energy. Panel (c) illustrates the variation of the magnetic moment for the same geometry. In the minimum, the magnetic moment is $0.4\mu_B$; further approach of the molecule towards the surface destroys the magnetic moment, whereas the dissociation towards the on-top sites (at $Z \sim 1.8$ Å) increases the magnetic moment because of the very limited charge transfer over the on-top site.

The second elbow plot shown in panel (b) corresponds to channel 4. This time the molecule has to pass a barrier before the atoms reach dissociatively the fcc hollow sites ($E = -1.65$ eV, $Z = 1.23$ Å). In this case the magnetic moment vanishes continuously along the reaction path, down to the nonmagnetic adsorption structure. In the exit channels, where the molecule is already dissociated, energy as well as magnetization are a function of height only, as one expects. In the same way, we investigated all fourteen channels. Figure 4 displays the variation of the PE at the bottom of all reaction channels as a function of the reaction coordinate s (= the distance from the starting point, measured along the path of minimum PE), beginning at a distance of 4 Å from the surface. Along channels 3 to 5, $3'$ to $4'$, 7,8 and 10 the dissociative adsorption of O_2 is a direct, strongly activated process with barriers varying between ~ 0.3 eV and ~ 1.5 eV. However, channels 2 and $2'$ suggest that the barrier might be lower along off-symmetry reaction paths.

C. Molecular precursor states

1. Structural and vibrational characterization

Along channels 1, 2, 6, $2'$, $6'$, we observe various local minima that can be identified with molecular precursors (see Table II). The minimum in the *t-b-t* channel 1 has already been discussed on the basis of Fig. 3. Comparison of channel 1 with the neighboring channels 2,$2'$ (shifted along the y axis) and 10,8,9 (corresponding to planar rotations over the bridge position) demonstrates that translation as well as ro-

tation lead to a rapid increase of the PE, so that this configuration corresponds to a real minimum on the 6D-PES with a molecule chemisorbed parallel to the surface in a *t-b-t* position.

Other local minima are identified in channels 2,2′ [nt-fcc(hcp)-nt] and 6,6′ [b-fcc(hcp)-*t*]. The energies are -0.18 to -0.27 eV/molecule for a position of the molecule parallel to the surface, at a height of $Z \simeq 1.84$ Å . For configurations 6 and 6′ the PE is not stationary with respect to a tilting of the molecule. A free minimization of the molecule starting from these t-fcc(hcp)-b configurations leads to the two essentially equivalent molecular precursor states described in Tables II and VI: an O_2 molecule stretched to $d = 1.43$ (1.42) Å is adsorbed close to the fcc (hcp) hollow, in a position oriented from top to bridge and slightly canted with respect to the surface plane, so that the end of the molecule over the surface atom is slightly higher. The parameter Δx in Table VI describes the lateral shift of the molecule out of the ideal hollow site towards the on-top position.

The adsorption energy is $E = -0.68$ (0.58) eV/molecule; compared to the configuration parallel to the surface, the molecule sinks somewhat deeper into the hollow, $z = 1.78$ (1.81) Å .

Hence our calculations support the conjecture[18,21,20] of the existence of two distinct but energetically almost degenerate chemisorbed molecular precursor states for O_2 on Pt (111). In the first state, the molecule is adsorbed in a symmetric *t-b-t* position characterized by a bond length of $d = 1.39$ Å and an O-O stretching frequency of $\nu_1 = 850$ cm^{-1} (see Table II). The predicted bond length is in good agreement with the experimental estimates based on NEXAFS ($d = 1.37$ Å , Ref. 26) and photoemission spectroscopy ($d = 1.39$ Å , Ref. 20). The stretching frequency is confirmed by various EELS measurements ($\nu_1 = 842$ cm^{-1}, Ref. 21; $\nu_1 = 875$ cm^{-1}, Ref. 18; $\nu_1 = 870$ cm^{-1}, Ref. 50). In the second state, the molecule sits in a slightly asymmetric *t*-fcc(hcp)-*b* position in a threefold hollow, with a bond-length of $d = 1.43$ (1.42) Å and a stretching frequency of $\nu_1 = 690$ (710) cm^{-1}. Again this is in good agreement with estimates based on photoemission spectroscopy ($d = 1.40$ Å, Ref. 51; $d = 1.43$ Å from core-level and $d = 1.47$ Å from valence-band spectra, Ref. 20) and EELS ($\nu_1 = 700$ cm^{-1}, Refs. 21 and 18; $\nu_1 = 710$ cm^{-1}, Ref. 50). From the curvature of the elbows in the *Z* direction we can derive also the lower metal-oxygen vibration frequencies ν_2. For this frequency ν_2 we get 340 (370) cm^{-1} for the *t*-fcc-*b*(*t-b-t*) precursor. Experimental EELS values have only been measured for the precursor over the bridge site ($\nu_2 = 380$ cm^{-1}, Ref. 18; $\nu_2 = 375$ cm^{-1}, Ref. 21) and agree well with our result. These adsorption sites agree in all details with a recent scanning-tunneling-microscopy study[28] (see also below).

2. Electronic and magnetic characterization

Our spin-polarized calculations also allow a characterization of the electronic and magnetic properties of the molecular precursors. Figures 5(a) and 5(c) show the isosurfaces of the difference electron densities and the spin density of the precursor in the *t-b-t* configuration. We find that charge flows from the substrate to the adsorbate and tends to fill the $\pi_\perp^\star$ antibonding states oriented perpendicular to the surface.

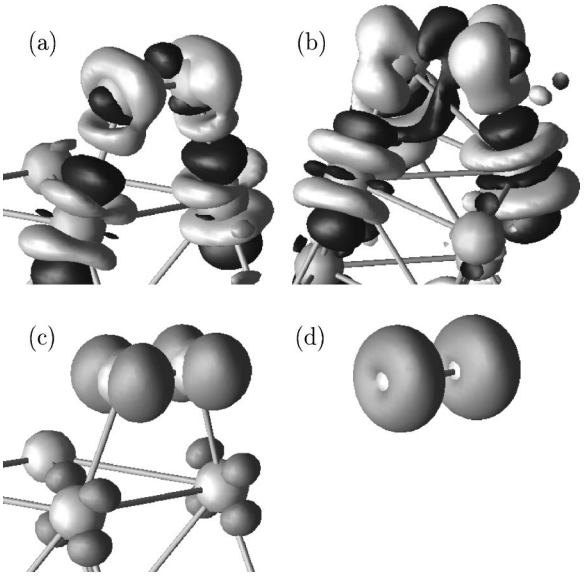

FIG. 5. Adsorption of O_2 on Pt(111): (a,b) Isosurfaces of the difference electron densities $(\rho[Pt(111)+O_2]-\rho[Pt(111)]-\rho(O_2))$ for (a) the superoxoprecursor in the *t-b-t* configuration and (b) the peroxoprecursor in the *t*-fcc-*b* configuration. Charge flows from the dark into the light regions. (c,d) Isosurfaces of the spin densities in (c) the superoxoprecursor and (d) the free O_2 molecule.

The filling of the $\pi_\perp^\star$ states but not the $\pi_\parallel^\star$ states is also corroborated by the analysis of the spin densities [Fig. 5(c)], which shows that the remaining magnetic moment of $m_{O_2} = 0.4\mu_B$ is carried by the $\pi_\parallel^\star$ states only, in contrast to the free O_2 molecule where the spin density is distributed homogeneously over both types of π states [see Fig. 5(d)]. Note that there is an induced magnetization of d_{xz} symmetry of the Pt atoms interacting with the adsorbate. The precursor in the *t*-fcc-*b* configuration, on the other hand, has no magnetic moment; the difference electron densities demonstrate an increased occupation of $\pi_\perp^\star$ and $\pi_\parallel^\star$ states [see Fig. 5(b)]. We also note an increased population of the Pt-*d* orbitals perpendicular to the Pt-O axis, due to redistribution effects. The adsorbate/substrate electron-transfer effects together with the redistribution within the substrate orbitals confirm the model of Feibelman[49] to explain the site preference observed in the O adsorption.

These general charge-transfer/redistribution effects are also confirmed by a detailed analysis of the local partial densities of states (Fig. 6). For the free O_2 molecule the lowest group of four eigenvalues corresponds to the spin-split bonding $ss\sigma(3\sigma_g)$ and $ss\sigma^\star(4\sigma_u)$ orbitals, whereas bonding $pp\sigma(5\sigma_g)$ and $pp\pi(1\pi_g)$ and antibonding $pp\pi^\star(2\pi_u)$ (the $5\sigma_g$ lies energetically between the spin-split $1\pi_g$) are distributed over an energy interval corresponding roughly to the width of the metal *d* band. The Fermi level falls into the gap between the spin-split $2\pi_u$ levels.

On adsorption in one of the molecular precursor states, both the bonding/antibonding and the exchange splitting of all states is reduced. For the *t-b-t* precursor a weak spin splitting of the $3\sigma_g$ and $4\sigma_u$ associated with the small magnetic moment is clearly recognizable, while for the nonmagnetic *t*-fcc-*b* precursor the spin splitting has completely dis-

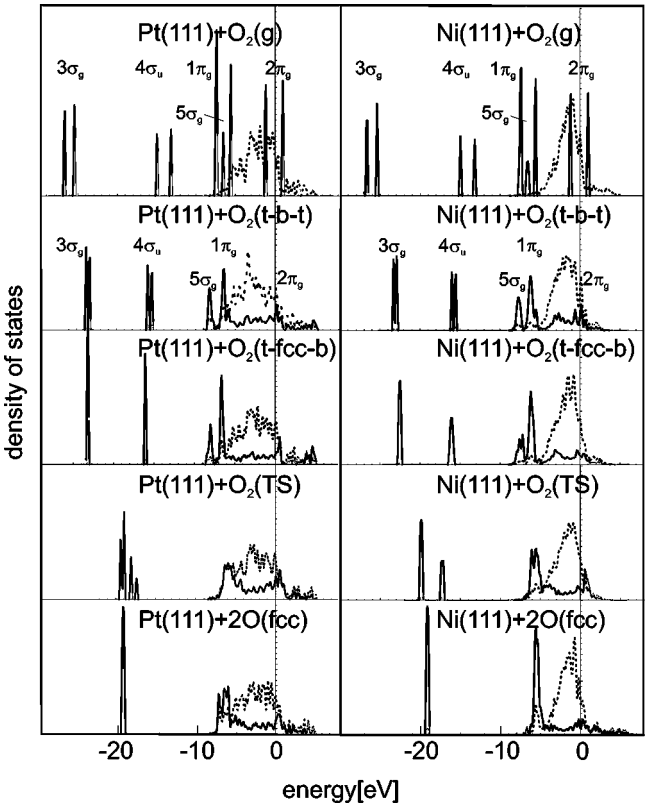

FIG. 6. Density of states for various states of oxygen adsorption on Pt(111) (left side) and Ni(111) (right side). Full lines, DOS projected on the O atom; broken lines, DOS projected onto the top layer of the substrate.

appeared. The *t*-fcc-*b* precursor also shows a slightly smaller bonding/antibonding splitting of the $ss\sigma$ states, corresponding to a more pronounced stretching of the molecule. The molecular orbitals derived from the atomic *p* states interact very strongly with the Pt-*d* band, in particular the more extended antibonding $2\pi_u$ states. The stronger interaction of the *t*-fcc-*b* precursor with the substrate causes a more pronounced broadening and a somewhat larger shift of these π states to lower binding energies and hence increasing population, in agreement with our analysis of the difference-electron densities. A further consequence of the reduced bonding/antibonding splitting of the π states is that the $5\sigma_g$ molecular orbital is now lower in energy than the $1\pi_g$.

The conclusions drawn on the basis of the charge and spin densities and of the local electronic DOS's are fully confirmed by the analysis of the STM images and the comparison with the experimental results of Stipe *et al.*[28]

3. Calculation of STM images

The availability of detailed STM images[28] of the precursor states has motivated us to attempt a calculation of the STM contrast. Constant current STM topographs are simulated by calculating the energy-resolved charge density $\rho(\vec{r},\epsilon)$ in the vacuum.[52] We evaluate isosurfaces of constant charge density $\rho(\vec{r},\epsilon)=C$ and determine the corrugation of these isosurfaces. Typically these isosurfaces are determined at an average distance of 3 Å from the core of the outermost atom. Although this is a much more simplified approach which is not expected to give quantitative agreement with the experiment, we are confident that qualitative features are well reproduced by this simple method.

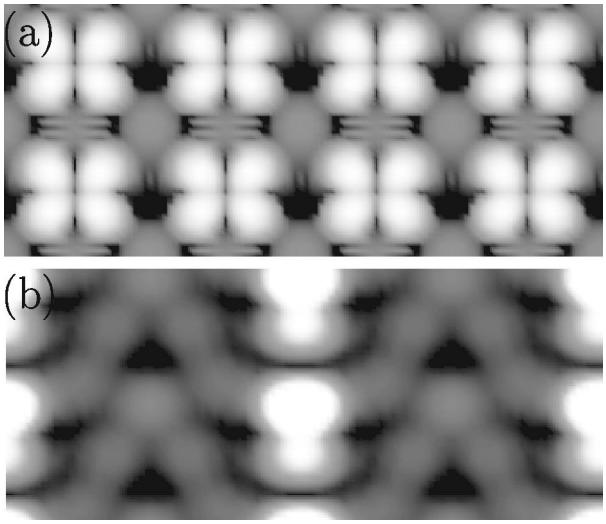

FIG. 7. Molecular precursors of O_2 on Pt(111): Calculated STM images for (a) the superoxoprecursor in the *t*-*b*-*t* configuration and (b) the peroxoprecursor in the *t*-fcc-*b* configuration; cf. text. For comparison with the experimental results, see Figs. 1 and 2 of Ref. 28.

For the visualization of the *t*-*b*-*t* precursor in Fig. 7 we show several supercells: the cell is doubled in the direction of the shorter axis and in the longer direction four cells are shown. The molecule itself is oriented as in channel 1 of Fig. 2, i.e., parallel to the long direction.

The superoxoprecursor in the flat *t*-*b*-*t* configuration is reproduced in the STM by an image with fourfold symmetry and minimum intensity in a plane perpendicular to the molecular axis, corresponding very well to the highest occupied molecular orbital with π^* symmetry.

For the second precursor state (*t*-fcc-*b*) we doubled our supercell already for the computation of the image in the longer (*x*) direction (see Fig. 2), so that in Fig. 7(b) four calculated cells are shown. Also in this case we can reproduce the slightly asymmetric ''pear-shaped'' charge-density distribution with the brighter feature on the top site for the *t*-fcc-*b* precursor. Also the depletions around the bridge lobe are in agreement with the STM study.

4. Barrier for rotation in a molecular precursor

This perfect agreement encouraged us to invest some effort in the determination of another property, which has been estimated on the basis of the discussed STM experiment. By raising the tunnel current, Stipe *et al.* succeeded in transforming the O_2 molecule residing in a *t*-fcc-*b* precursor into an equivalent one rotated by 30°. The barrier related to this rotation has been estimated to be 150–175 meV.[53]

This rotation corresponds to a change from channel 6 via 2 back into a rotated version of 6. Because of the low symmetry at this site, inducing a tilting of the molecule and a shift of the center of mass during the rotation, we used the NEB method explained in Sec. III. The calculated barrier height of 150 meV is in good agreement with the experimental estimate; for a more accurate value, substrate effects have to be included.

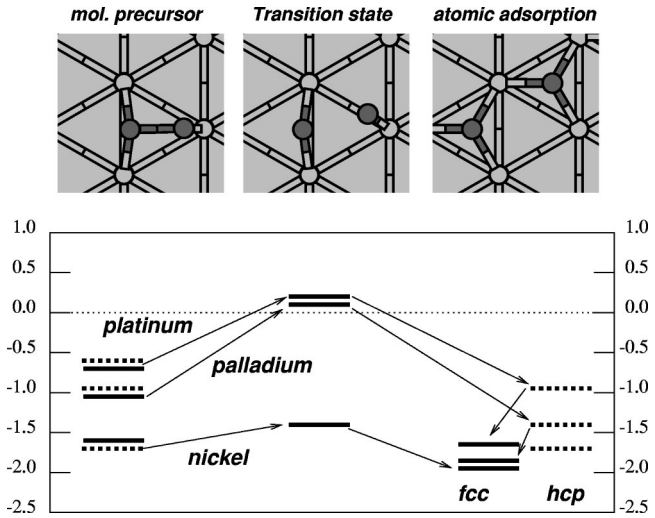

FIG. 8. Sketch of the initial, transition, and final states for the dissociative adsorption of O_2 over nickel, palladium, and platinum(111). The initial state is the precursor over the hollow position [fcc (solid line) for Pt and Pd, hcp (dashed lines) for Ni] and then O_2 dissociated via the transition state (for an exact characterization of the geometry see Table VI) into the again hollow adsorbed oxygen atoms [fcc (solid line) for all surfaces; for palladium and platinum the hcp site (dashed line) has to be crossed].

D. Dissociation

Within the reaction channels defined above, both precursors are separated by a substantial barrier from the dissociated chemisorbed atomic state. A realistic scenario for finding a lower barrier is *t*-*b*-*t* to nt-hcp-nt to fcc-nt-fcc (i.e., a parallel shift of the atom in the *y* direction, switching consecutively from channel 1 to channel 2, 3, and finally 4, cf. Figs. 4 and 2), or into the other direction into the fcc hollows, followed by a subsequent diffusion into the hcp-hollow sites. Rotation in the intermediate nt-hollow-nt configuration can transform the *t*-*b*-*t* precursor with only a small barrier (compare the preceding section) into the *t*-hollow-*b* precursor.

For the *t*-hcp(fcc)-*b* precursor, rotation to nt-hcp(fcc)-nt leads into the same reaction path. In both cases, we find from the results given in Fig. 4 a barrier at about $E=0.18$ eV relative to the free molecule. In order to allow also for less symmetric intermediate positions along the reaction path, we used the NEB method for the determination of the transition state along *t*-fcc-*b* and two hcp-adsorbed oxygen atoms. The result is sketched schematically in Fig. 8. For the lowest transition state [within the $c(2\times4)$ cell] the O atom near the bridge site crosses it, while the second atom rotates around the top atom passing asymmetrically the second bridge. A more detailed characterization of the transition state can be found in Table VI. The physical principle determining the transition state is evidently to avoid the breaking of adsorbate/substrate bonds during the reaction. However, the barrier along this pathway agrees with the previous estimates from the elbows.

Hence our calculations predict that the barrier for a dissociation of the molecular precursor is higher than for its desorption. Experimentally, the dissociation barrier has been estimated to be slightly lower than the desorption barrier, at least for low coverages.[23] However, our result agrees with the postulate of high kinetic barriers for the associative desorption of O in the high coverage regime.[22] One has to remember that the saturation coverage for atomic oxygen due to dissociative adsorption of O_2 is only 0.25 ML,[54] while the dissociative adsorption of NO_2 followed by NO desorption can form oxygen layers with coverages up to 0.75 ML.[22] This means that at the investigated coverage a higher barrier for dissociation than for desorption is in agreement with the experimental findings. The local DOS at the TS shown in Fig. 6 demonstrates the further reduction of the bonding/antibonding splitting of all orbitals. Interestingly, a weak spin splitting reappears.

TABLE III. Atomic adsorption oxygen at the high symmetry sites of Ni(111) at $\Theta=0.25$ ML: adsorption energy E (eV) (with respect to half a free oxygen molecule), distance Z (Å) to the surface, distance $d_{\text{O-Ni}}$ (Å) to the nearest Ni atom, magnetic moments of the oxygen atom m_O and of the neighboring Ni atom m_{Ni}, and work-function change due to oxygen adsorption. The experimental values are taken from Refs. 31,30, and 32.

		Top	Bridge	fcc	hcp	Expt.
E	(eV)	−0.48	−1.77	−2.32	−2.20	−2.28
Z	(Å)	1.68	1.29	1.16	1.17	1.17
$d_{\text{O-Ni}}$	(Å)	1.68	1.79	1.86	1.86	1.85
m_O	(μ_B)	0.43	0.18	0.13	0.09	
m_{Ni}	(μ_B)	0.7	0.6	0.56	0.6	
$\Delta\Phi$	(eV)	1.6	0.4	0.8	0.8	0.8

V. OXYGEN ON NICKEL(111)

For the investigation of the O_2-Ni system we chose a slightly different strategy. Since we expect a qualitatively similar adsorption behavior, we calculated only a few elbow scans to confirm our assumption. Therefore, we did a more detailed investigation for the atomic adsorption and the dissociation pathways.

A. Atomic adsorption

To determine the energetically most favorable adsorption site, we relaxed the oxygen atoms in several high-symmetry sites for a $p(2\times2)$ superstructure. The results are compiled in Table III: adsorption in fcc-hollow positions leads to an energy [with respect to $\frac{1}{2}E(O)_2$] of $E=-2.32$ eV/atom, energetically only slightly more favorable than for adsorption in the hcp hollow ($E=-2.20$ eV/atom), while adsorption in bridge ($E=-1.77$ eV/atom) and on-top sites ($E=-0.48$ eV/atom) has much lower adsorption energies. This confirms the usual trend of oxygen to occupy high coordinated sites and agrees well with the microcalorimetric measurements of Stuckless *et al.*[31] of 440 kJ/mol (O_2) ($E=2.28$ eV/atom).

In the hollow positions the atom is closest to the surface ($Z^{\text{fcc}}=1.16$ Å , $Z^{\text{hcp}}=1.17$ Å) resulting in a nickel-oxygen distance of $d_{\text{O-Ni}}=1.86$ Å [NEXAFS (Ref. 30): $d_{\text{O-Ni}}=1.85\pm0.05$ Å]. Also, our prediction for the work-function change of $\Delta\Phi=+0.8$ eV is in nice agreement with experiment.[32] The magnetic moment of the free O atom is reduced upon adsorption. This reduction depends on the distance from the nearest Ni atoms and on the O-Ni coordina-

TABLE IV. Atomic adsorption of two oxygen atoms in hollow positions of a nickel (111) surface at $\Theta=\frac{1}{2}$ ML in two configurations A,B (cf. text): energy E (eV), distance from the surface Z (Å), and magnetic moment m_O/atom.

		fcc (A)	fcc (B)	hcp (A)	hcp (B)
E	(eV)	1.91	1.88	1.77	1.75
Z	(Å)	1.12	1.12	1.13	1.15
m_O	(μ_B)	0.1	0.1	0.1	0.1

tion number: it is smallest for top-site adsorption and strongest for adsorption in the hcp hollow where only a moment of $m_O=0.09\mu_B$ subsides.

Since we used the $c(2\times4)$ cell depicted in Fig. 2 for the molecular adsorption, we also investigated the resulting higher oxygen coverage of half a monolayer (see Table IV). within this cell two inequivalent arrangements of hollow adsorbed O atoms are possible: in the first case the oxygen atoms form chains parallel to the shorter axis of the cell (A) separated by 5.00 Å , whereas for the second possibility the chains are parallel to the longer axis (B) and separated by only 4.33 Å . The distances for nearest-neighbor oxygen atoms are in both cases the same.

The height above the surface is very similar to the lower coverage case for the fcc hollow ($Z^A=Z^B=1.12$ Å) as well as for the hcp site ($Z^A=1.13$ Å , $Z^B=1.15$ Å). The change in the adsorption energy is much more pronounced (cf. Tables III and IV). However, the energy difference between fcc and hcp adsorption remains nearly unchanged, and also the difference between arrangements A and B is only rather small (<50 meV).

Figure 6 shows the partial density of states (DOS) of the adsorbed oxygen atom, where a very strong adsorbate-substrate bond is manifested by a pronounced peak around $E=-6$ eV. The adsorption-induced charge flow, depicted in Fig. 10, illustrates nicely the argument for the preference of the fcc- over the hcp-hollow site, discussed in Sec. IV. During adsorption, the O atom becomes charged and the resulting repulsion of electrons leads to a charge redistribution at the substrate.

B. Potential-energy surface

Figure 9 shows the energy as a function of the distance from the surface for the two elbow scans leading in the case of O_2/Pt(111) to molecular precursor states: at large distances from the surface, the influence of the surface is quite small. From a height of about 2.6 Å above the surface the energy decreases and the oxygen molecule becomes elongated. Finally in both cases there is a minimum in the energy curve indicating molecular precursors (for the t-b-t pathway at a height of about $Z=1.8$ Å and for the precursor over the hollow at $Z\simeq1.6$ Å).

These local minima are exactly equivalent to those determined on the platinum surface, which justifies our assumption of a similar PES.

C. Molecular precursor states

1. Structural characterization

Table VI gives the comparison of the three precursor states similar to those found on the platinum surface: over

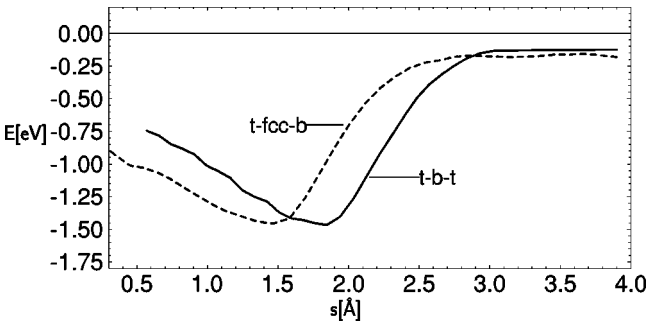

FIG. 9. Potential energy for O_2 on Ni(111). Variation of the potential energy along the bottom of the reaction channels 1 (t-b-t) and 6 (t-fcc-b) defined in Fig. 2 and in the text. The reaction coordinate s measures the distance from the starting point 4 Å above the surface plane along the deepest points in each channel.

the bridge site oriented towards the substrate atoms (t-b-t), over the hollow sites connecting bridge and on-top sites [t-fcc(hcp)-b].

In contrast to platinum where we had found a difference of 0.1 eV for precursor adsorption in the fcc and hcp hollows, on nickel the precursor states over the hollow positions are very similar: energetically both are nearly degenerate ($E^{t\text{-fcc-}b}=-1.65$ eV, $E^{t\text{-hcp-}b}=-1.67$ eV), with even a slight preference of the hcp hollow. The distance from the surface is 1.62 Å for both precursors, the O_2 bond length $d=1.46$ Å (t-hcp-b) and $d=1.47$ Å (t-fcc-b), respectively, and the axis of the molecule is tilted by 10° with respect to the surface plane. Also, the magnetic moments of the oxygen molecule are equal, $m_{O_2}=0.2\mu_B$ per molecule.

The precursor state over the bridge site is higher in energy ($E^{t\text{-}b\text{-}t}=-1.41$ eV). In this site, the oxygen bond is therefore less strained ($d=1.42$ Å) and also the magnetic moment is still higher ($m_{O_2}=0.4\mu_B$). The height above the surface is $Z=1.77$ Å . Again the difference of 0.26 eV in the energies of the t-hcp-b and t-b-t precursors is remarkable compared to the much smaller difference of only 0.04 eV (t-fcc-b and t-b-t) found for O_2 on Pt. We shall return to this point below.

2. Electronic and magnetic characterization

The LDOS's of the different adsorption sites (Fig. 6) show in principle the same features as the O_2/Pt system. Characteristic differences with respect to O_2/Pt are discussed in Sec. VII. Also charge-redistribution effects are very similar to the adsorption system discussed previously. In the case of the nickel surface it leads to a slight reduction of the surface magnetic moment.

3. Dissociation

The final step in our description of the adsorption process is the calculation of the energy barriers to the dissociation. Using the same strategy as for platinum, we calculated dissociation pathways for the t-hcp-b and the t-b-t precursor; for these calculations we have neglected the small differences between the two hollow sites. For the t-b-t precursor state the NEB calculations show that there is no barrier for a transformation of the t-b-t into the t-hcp-b precursor by a rotation about a vertical axis combined with a small shift of

the center of gravity of the molecule. This indicates that the minimum in the PES corresponding to the *t*-*b*-*t* state is a saddle point, rather than a true local minimum.

The energetically most favorable path for dissociation starting from the *t*-hcp-*b* precursor is very similar to that on the platinum surface shown in Fig. 8. Initially the molecule is rotated, leading to an increase of energy; at the transition state both oxygen atoms are located near bridge sites. The energy at the transition state is only 0.2 eV higher than in the precursor. After crossing the transition state, the energy decreases steeply to the value of coadsorbed O atoms. At the transition state the height above the surface of the oxygen molecule (bond length $d=1.81$ Å) decreases to $Z=1.49$ Å and also the tilting angle decreases to 8°.

The barrier height is in reasonable agreement with the estimate of $\Delta E_{\mathrm{barr}}=70$–$100$ meV by Beutl *et al.*[33] from molecular-beam experiments. However, one has to keep in mind that the experimental results are for the low-coverage case.

An analysis of the local density of states shows a reduced splitting of both the binding $3\sigma_g$ and the antibonding $4\sigma_u$ state ($E_B=-20$ eV and -17 eV, respectively) and the 1π and the $5\sigma_g$ state ($E_B=-6$ eV) compared to the precursor state, indicating the tendency towards the atomic behavior.

VI. OXYGEN ON PALLADIUM (111)

In order to establish clear trends in the mechanism for oxygen adsorption on the platinum group metals, we extended our calculations also to palladium.

Because of the similarity in the lattice constants of Pt ($a=3.99$ Å) and Pd ($a=3.96$ Å), we use the geometries for the oxygen-platinum system as a starting point for the relaxation calculations. The energy gain during the structural optimization is less than 30 meV for the molecular precursor states as well as for atomic adsorption. This makes us confident that the transition state of the O_2-Pt system is a very good approximation for the transition state over the Pd(111) surface. However, we have checked this assumption by an independent transition state search leading to a barrier height 30 meV lower than that at the fixed O_2:Pt(111) geometry. So we have demonstrated that it is a justified assumption to transfer adsorption/transition state geometries between similar adsorption systems.

The structural and energetic data of the molecular precursor states, the transition state for dissociation, and the final atomic adsorption are summarized in Table VI. As expected, O_2/Pd(111) behaves much more like oxygen on Pt than like oxygen on nickel: there is a pronounced preference for the fcc over the hcp hollow for both precursor and atomic adsorption; the dissociation barrier is slightly higher than the desorption barrier.

Since there have been predictions based on electron-energy-loss spectroscopy[34] of three different chemisorbed molecular precursors for O_2/Pd(111), we calculated the frequencies for the molecular and atomic adsorption structures on the surface (see Table V), so that we can relate the precursor states to the experimentally postulated ones. We calculated the complete dynamical matrix for the two oxygen atoms by finite displacements and solved the corresponding eigenvalue problem. For the two atomic structures in the hollow sites, we get metal-oxygen stretching frequencies of 490 cm^{-1} (460 cm^{-1}) for the fcc (hcp) case, compared to an experimental value 485 cm^{-1} at $\Theta=0.25$ ML.

TABLE V. Frequencies of oxygen adsorbed on Pd(111) at $\Theta_O=0.5$ in comparison with experiment: intramolecular stretch frequency ν_1 and corresponding experimental values ν_1^{exp}, antisymmetric (symmetric) oxygen-metal vibrational frequency ν_2 ($\bar{\nu}_2$) in wave numbers. The experimental data are taken from Ref. 34.

	t-*b*-*t*	*t*-fcc-*b*	*t*-hcp-*b*	fcc	hcp
ν_1	960	890	830		
ν_1^{exp}	1035	850		485	
ν_2	480	440	450	490	460
$\bar{\nu}_2$	390	380	320		

The intramolecular stretching frequencies of the molecular states have been measured at 1035 cm^{-1} and 850 cm^{-1} and an additional peak has been found at 650 cm^{-1}. This lowest peak is nearly invisible for low temperatures, but increases in intensity upon heating like the peak at 850 cm^{-1}, while the intensity of the highest peak decreases.

According to our calculations, the highest peak can be attributed to the *t*-*b*-*t* precursor ($\nu=960$ cm^{-1}), which is transformed into the *t*-fcc(hcp)-*b* state upon heating ($\nu=890$ cm^{-1} and 830 cm^{-1}, respectively), corresponding to the peak at 850 cm^{-1} from the experiment.

None of the states we calculated could be related to the loss feature at 650 cm^{-1}, which has to be left to a more complete examination of the PES.[14] However, according to our experience with the O_2-Pt(111) PES and the similarity of the systems, we do not exclude the possibility of an adsorption at steps.

VII. DISCUSSION AND COMPARISON

Several factors determine the trends in the adsorption behavior of O on the Pt-group metals: The dominant contribution is the chemical reactivity determining the strength of the metal-adsorbate bonds. According to a reactivity model introduced by Hammer and Nørskov,[55] this reactivity is mainly determined by the position of the center of the metal *d* band relative to the Fermi level and hence also relative to the lowest unoccupied (antibonding) molecular orbitals (LUMO). For the surfaces discussed in this paper, the center of the *d* bands of the surface atoms is located at -1.98 eV for platinum, -1.54 eV for palladium, and -1.52 (-0.81) for the majority (minority) band of nickel (average *d*-band center -1.21 eV). Already at a first glance the correlation between these values and the trends in both the molecular and atomic adsorption energies is obvious.

The main electronic effects dominating during the adsorption can be traced on the basis of the local density of states (LDOS) (Fig. 6). During adsorption, the spin polarization decreases and the bonding/antibonding splitting is reduced, effects which have been discussed in detail previously. They are more pronounced for nickel than for platinum and for the *t*-fcc-*b* precursor than for the *t*-*b*-*t* state and directly correlated with the bond length of the O_2 molecule in relation to the interatomic distances on the substrate. The second and by

TABLE VI. Comparison of various O_2 states on Ni, Pd, and Pt(111): energy E with respect to the free O_2 molecule, height Z (Å) above the surface, bond length d (Å), lateral distance of the center of mass of the molecule from the next high-symmetry site Δx (Å), inclination with respect to the surface plane Θ (in degrees) and magnetic moment m_{O_2} (μ_B).

State	Surface	E (eV)	Z (Å)	d (Å)	Δx (Å)	Θ (deg)	m_{O_2} (μ_B)
t-fcc-*b*	Ni(111)	−1.65	1.62	1.47	0.18	10	0.2
	Pd(111)	−1.01	1.75	1.39	0.18	11	0
	Pt(111)	−0.68	1.78	1.43	0.21	10	0
t-hcp-*b*	Ni(111)	−1.67	1.62	1.46	0.15	10	0.2
	Pd(111)	−0.92	1.79	1.41	0.23	9	0
	Pt(111)	−0.58	1.81	1.42	0.23	8	0
t-*b*-*t*	Ni(111)	−1.41	1.77	1.42	0	0	0.4
	Pd(111)	−0.89	1.91	1.36	0	0	0.3
	Pt(111)	−0.72	1.92	1.39	0	0	0.4
TS	Ni(111)	−1.45	1.49	1.81	0.20	8	0.2
	Pd(111)	0.10	1.58	2.15	0.32	9	0.9
	Pt(111)	0.18	1.60	2.06	0.33	8	0.3
2×fcc	Ni(111)	−1.90	1.12				
	Pd(111)	−1.87	1.19				
	Pt(111)	−1.65	1.23				
2×hcp	Ni(111)	−1.76	1.14				
	Pd(111)	−1.44	1.21				
	Pt(111)	−0.98	1.25				

far dominant contribution to the adsorption process is the interaction between the antibonding $2\pi_u$ orbital (HOMO) and the metal *d* band. The energy related to this hybridization is approximately proportional to the inverse of the difference in energy between the HOMO and the metal band.[4] Neglecting spin splitting, the $2\pi_u$ orbital is located at the Fermi level, the metal *d* bands at the previously mentioned positions. This relation explains nicely the trend for the molecular precursor states.

At the transition state (fourth panel in Fig. 6), the change in the molecular orbitals leading to dissociation indicates a different character of the transition state on Pt than on Ni. In contrast to the precursor states at the transition state, the splitting between the $3\sigma_g$ and $4\sigma_u$ is smaller for platinum than for nickel and also the bond length on platinum is longer (see Table VI). This means that the molecular bond has to be more stretched over Pt, until the metal-adsorbate bond is strong enough to break the molecular bond. This is a consequence of the much smaller lattice constant of nickel, which allows the formation of a stronger adsorbate/substrate bond already at a smaller stretching of the O-O bond. The dominant influence of the lattice constant is the reason for the rather similar absolute values of the transition-state energies over Pd and Pt, while that over Ni is much lower.

Finally, the dissociation is complete, and oxygen is adsorbed in atomic form. In the lowest panel of the LDOS there is only a single *s* peak for the oxygen and the *p* states are [now nearly completely filled; cf. Fig. 10(a)] hybridized with the metal *d* band. The adsorption height follows the trend in the energies and not—as one could naively expect—the trends in the lattice constants. As for the molecular precursors, the trend in the atomic adsorption energies can be related to the *d*-band centers: the stronger the bond energy, the lower the height.

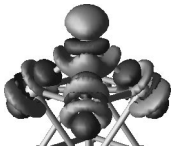

FIG. 10. Isosurfaces of the difference electron densities $(\rho[\mathrm{Ni}(111)+\mathrm{O}_2]-\rho(\mathrm{Ni}(111))-\rho(\mathrm{O}_2))$ for the atomic adsorbed oxygen in an fcc-hollow site. Charge flows from the dark into the light regions.

Summarizing, we can say that the trend in the adsorption energies can be explained by the variation of the *d*-band centers, while the transition state is also determined by geometrical factors such as the lattice constant. This interplay leads to the highest relative barrier (out of the precursor state) for Pd, followed by Pt and only a small barrier for Ni (see Fig. 8). These trends can be observed exactly in the sticking curves in Fig. 1: The sticking coefficient for high translational energies follows the general trend of the chemical reactivities from Ni over Pd to the lowest sticking probability for Pt. (The absolute sticking values may not be exactly comparable, since they have been obtained by different groups and the determination of sticking coefficients is an experimentally very difficult task [see, e.g., the different experiments for H_2 on Pd(111)], but the general trends are visible.) In contrast to that, the minima of the sticking curves (at ~30 meV for Ni, ~120 meV for Pt, and ~200 meV for Pd) follow a different trend, being determined by the barrier height to dissociation, which is highest for Pd. The exact determination of the barriers for the low-coverage case is rather difficult from our calculations, since at this high coverage ($\Theta_O = 0.5$ ML) there are in addition to chemical and geometric also kinetic contributions to the barriers, due to sterical hindering by neighboring molecules.[22]

The slope of the increase in the sticking curves is influenced by the distribution of the barriers:[56] in a simplified picture a high corrugation (i.e., a high variation of barrier heights) leads to a shallow increase of the sticking with energy, while the steep increase for O_2 on Ni indicates a small corrugation. To probe this prediction, we calculated the barrier height in the *b*-*t*-*b* channel, which is among the highest dissociation barriers also over Pd and Ni, by taking the O_2:Pt(111) geometry of the barrier. The results are $E_{\mathrm{barr}}(b\text{-}t\text{-}b) = -0.77$ eV for Ni, 0.91 eV for Pd, and 1.29 eV for Pt (cf. Fig. 4). The difference between these values and the energy of the transition state from Table VI should be a reasonable estimate for the corrugation of the three surfaces and gives $\Delta E_{\mathrm{barr}} = 0.7$ eV, 0.8 eV, and 1.1 eV for Ni, Pd, and Pt, respectively. Indeed we find the largest corrugation for the Pt surface, followed by Pd and finally nickel, which is the flattest of the three, in agreement with the trend of the slopes of the sticking curves. For nickel the assumption of similar geometries is eventually not so well justified, due to the difference in lattice constants, so that the corrugation will be even lower, which agrees well with the results of Beutl *et al.*[33] that the influence of rotations of the molecule on the adsorption process is very small. However, for a more complete discussion of the dynamics of the adsorption process,

molecular-dynamics simulations based on the calculated potential energy surfaces are necessary.[57] Based on the calculated potential-energy surface, such a study is in progress for the adsorption/dissociation process on platinum(111).[58]

VIII. CONCLUSION

In conclusion, we can say that the trends for O_2 adsorption are determined by the following factors.

(i) A *chemical* contribution, determined by the location of the metal *d* band. This is the dominant part and determines especially the adsorption energies and the absolute sticking coefficient.

(ii) The *geometrical* influence of the different lattice constants, which determines how far the molecular bond has to be stretched, so that the metal-oxygen bonding is strong enough to break the molecular bond, and therefore has the largest influence at the transition state.

(iii) *Kinetical* contributions at high coverage originating from the sterical hindering of neighboring molecules, which are absent if the molecules are farther apart and make an extrapolation from our results to the low-coverage regime difficult. The interplay between the chemical and geometrical contributions leads to a different trend of the relative barrier heights, which is manifested in the positions of the minimum in the sticking curves (Fig. 1). The corrugation of the potential-energy surface determines the slope of the rise in sticking for higher translational energies and follows the same trend as the adsorption energies.

ACKNOWLEDGMENTS

This work has been supported by the Austrian Science Funds under Project No. S8106-PHY. The calculations have been performed mainly on the Cray T3E at the John von Neumann Institute for Computing in the Forschungszentrum Jülich.

[1] G. Somorjai, *Introduction to Surface Chemistry and Catalysis* (Wiley, New York, 1994).
[2] A. Eichler, G. Kresse, and J. Hafner, Surf. Sci. **397**, 116 (1998).
[3] A. Eichler, G. Kresse, and J. Hafner, Phys. Rev. Lett. **77**, 1119 (1996).
[4] B. Hammer and J. K. Nørskov, Surf. Sci. **343**, 211 (1995).
[5] A. Eichler and J. Hafner, Phys. Rev. Lett. **79**, 4481 (1997).
[6] P. A. Gravil, D. M. Bird, and J. A. White, Phys. Rev. Lett. **77**, 3933 (1996).
[7] A. Eichler and J. Hafner, Phys. Rev. B **57**, 10 110 (1998).
[8] A. Eichler and J. Hafner, J. Chem. Phys. **109**, 5585 (1998).
[9] B. Hammer, Y. Morikawa, and J. K. Nørskov, Phys. Rev. Lett. **76**, 2141 (1996).
[10] A. Groß, S. Wilke, and M. Scheffler, Phys. Rev. Lett. **75**, 2718 (1995); S. Wilke and M. Scheffler, Phys. Rev. B **53**, 4926 (1996).
[11] A. Eichler, J. Hafner, A. Groß , and M. Scheffler, Phys. Rev. B **59**, 13 297 (1999); Chem. Phys. Lett. **311**, 1 (1999).
[12] C. Stampfl, H. J. Kreuzer, S. H. Payne, H. Pfnür, and M. Scheffler, Phys. Rev. Lett. **83**, 2993 (1999).
[13] K. D. Renudlic and A. Winkler, Surf. Sci. **299/300**, 261 (1994).
[14] K. Honkala and K. Laasonen (unpublished).
[15] S. Y. Liem, J. H. R. Clarke, and G. Kresse (unpublished).
[16] F. Mittendorfer, A. Eichler, and J. Hafner, Surf. Sci. **433-435**, 756 (1999).
[17] J. Grimblot, A. C. Luntz, and D. E. Fowler, J. Electron Spectrosc. Relat. Phenom. **52**, 161 (1990).
[18] H. Steininger, S. Lehwald, and H. Ihbach, Surf. Sci. **17**, 342 (1982).
[19] W. Ranke and H. J. Kuhr, Phys. Rev. B **39**, 1595 (1989).
[20] C. Puglia, A. Wilsson, B. Hernnäs, O. Karis, P. Bennich, and N. Martensson, Surf. Sci. **342**, 119 (1995).
[21] N. R. Avery, Chem. Phys. Lett. **96**, 371 (1983).
[22] D. H. Parker, M. E. Bartram, and B. E. Koel, Surf. Sci. **217**, 489 (1989).
[23] A. C. Luntz, M. D. Williams, and D. S. Bethune, J. Chem. Phys. **89**, 4381 (1988); A. C. Luntz, J. Grimblot, and D. E. Fowler, Phys. Rev. B **39**, 12 903 (1989).
[24] J. Stöhr, J. L. Gland, W. Eberhardt, D. Outka, R. J. Madix, F. Sette, R. J. Koestner, and U. Doebler, Phys. Rev. Lett. **51**, 2414 (1983).
[25] D. A. Outka, J. Stöhr, W. Jark, P. Stevens, J. Solomon, and R. J. Madix, Phys. Rev. B **35**, 4119 (1987).
[26] W. Wurth, J. Stöhr, P. Feulner, X. Pan, K. R. Bauchspiess, Y. Baba, E. Hudel, G. Rocker, and D. Menzel, Phys. Rev. Lett. **65**, 2426 (1990).
[27] N. Materer, U. Starke, A. Barbieri, R. Döll, K. Heinz, M. A. Van Hove, and G. A. Somorjai, Surf. Sci. **325**, 207 (1995).
[28] B. C. Stipe, M. A. Rezaei, W. Ho, S. Gao, M. Persson, and B. I. Lundqvist, Phys. Rev. Lett. **78**, 4410 (1997).
[29] M. A. Mendez, W. Oed, A. Fricke, L. Hammer, K. Heinz, and K. Müller, Surf. Sci. **253**, 99 (1991).
[30] M. Pedio, L. Becker, B. Hillert, S. D'Addato, and J. Haase, Phys. Rev. B **41**, 7462 (1991).
[31] J. T. Stuckless, C. E. Wartnaby, N. Al-Sarraf, St. J. B. Dixon-Warren, M. Kovar, and D. A. King, J. Chem. Phys. **106**, 2012 (1996).
[32] D. F. Mitchell and M. J. Graham, Surf. Sci. **114**, 546 (1982).
[33] M. Beutl, K. D. Rendulic, and G. R. Castro, Surf. Sci. **385**, 97 (1997).
[34] R. Imbihl and J. E. Demuth, Surf. Sci. **173**, 395 (1986).
[35] P. Sjövall and P. Uvdall, Chem. Phys. Lett. **89**, 355 (1998).
[36] G. Kresse and J. Hafner, Phys. Rev. B **47**, R558 (1993); **48**, 13 115 (1993).
[37] G. Kresse and J. Furthmüller, Phys. Rev. B **54**, 11 169 (1996); Comput. Mater. Sci. **6**, 15 (1996).
[38] E. G. Moroni, G. Kresse, J. Hafner, and J. Furthmüller, Phys. Rev. B **56**, 15 629 (1997).
[39] J. P. Perdew, J. A. Chevary, S. H. Vosto, K. A. Jackson, M. R. Pederson, D. J. Singh, and C. Frolhais, Phys. Rev. B **46**, 6671 (1992).
[40] D. Vanderbilt, Phys. Rev. B **41**, 7892 (1990); G. Kresse and J. Hafner, J. Phys.: Condens. Matter **6**, 8245 (1994).
[41] P. E. Blöchl, Phys. Rev. B **50**, 17 953 (1994).
[42] G. Kresse and D. Joubert, Phys. Rev. B **59**, 1758 (1999).

[43] A. Eichler, J. Hafner, and G. Kresse, J. Phys.: Condens. Matter **8**, 7659 (1996).
[44] F. Mittendorfer, A. Eichler, and J. Hafner, Surf. Sci. **423**, 1 (1999).
[45] M. Methfessel and A. Paxton, Phys. Rev. B **40**, 3616 (1989).
[46] G. Mills, H. Jónsson, and G. K. Schenter, Surf. Sci. **324**, 305 (1995).
[47] A. Ulitsky and R. Elber, J. Chem. Phys. **92**, 1510 (1990).
[48] A. Eichler and J. Hafner, Phys. Rev. B **59**, 5960 (1999).
[49] P. J. Feibelman, Phys. Rev. B **56**, 10 532 (1997).
[50] J. L. Gland, B. A. Sexton, and G. B. Fisher, Surf. Sci. **95**, 587 (1980).
[51] W. Eberhardt, T. Upton, S. Cramm, and L. Incoccia, Chem. Phys. Lett. **146**, 561 (1988).
[52] J. Tersoff and D. R. Hamann, Phys. Rev. Lett. **50**, 1998 (1985); Phys. Rev. B **31**, 805 (1985).
[53] B. C. Stipe, M. A. Rezaei, and W. Ho, Science **279**, 1907 (1998).
[54] P. R. Norton, J. A. Davies, and T. E. Jackman, Surf. Sci. **122**, L593 (1982).
[55] B. Hammer and J. K. Nørskov, in *Chemisorption and Reactivity on Supported Clusters and Thin Films* (Kluwer Academic Publishers, Dordrecht, 1997), p. 285.
[56] A. Groß , B. Hammer, M. Scheffler, and W. Brenig, Phys. Rev. Lett. **73**, 3121 (1994).
[57] A. Eichler, J. Hafner, A. Groß , and M. Scheffler, Phys. Rev. B **59**, 13 297 (1999).
[58] A. Groß , A. Eichler, J. Hafner, F. Kirchhoff, M. J. Mehl, and D. A. Papaconstantopoulos (unpublished).